Ocean Engineering 274 (2023) 114034

Contents lists available at ScienceDirect

Ocean Engineering

journal homepage: www.elsevier.com/locate/oceaneng

Technical note

An experimental comparison of Deep Learning strategies for AUV navigation in DVL-denied environments

Edoardo Topini [a,b,*], Francesco Fanelli [c], Alberto Topini [a,b], Miles Pebody [c], Alessandro Ridolfi [a,b], Alexander B. Phillips [c], Benedetto Allotta [a,b]

[a] Department of Industrial Engineering, University of Florence, via di Santa Marta 3, Florence, 50139, Italy
[b] Interuniversity Center of Integrated Systems for the Marine Environment (ISME)[1], Italy
[c] National Oceanography Centre (NOC), European Way, Southampton, SO14 3ZH, United Kingdom

ARTICLE INFO

Keywords:
Autonomous Underwater Vehicles
Deep Learning
Marine robotics
Navigation strategies

ABSTRACT

Accurate and robust navigation and localisation systems are critical for Autonomous Underwater Vehicles (AUVs) in order to perform missions in challenging environments. However, since the Global Positioning System (GPS) is not available in the underwater domain, the localisation task is commonly fulfilled by integrating direct linear speed readings provided by a Doppler Velocity Log (DVL) over time. As a consequence, DVL failures or fallacies and DVL-denied environments may arise as unexpected causes for severe malfunctions of the whole navigation system. Motivated by these considerations and the outstanding performance of Deep Neural Networks (DNNs) in supervised regression problems, a Deep Learning (DL) -based approach has been developed to estimate the vehicle's body-frame velocity, without canonically employing DVL measurements, in a Dead-Reckoning (DR) navigation strategy. In particular, this work will describe the whole framework, starting from the data gathered by the AUVs of the National Oceanography Centre (NOC) during different field campaigns, through to the data pre-processing and the inference of the predicted velocity. Finally, a comprehensive offline comparison between different DL-based models is presented to assess the validity of the proposed approach.

1. Introduction

The interest in Autonomous Underwater Vehicles (AUVs) has significantly increased in the last decades. The possibility of replacing humans with robots in such a dangerous and challenging scenario has led the field of AUV applications to spread from the military to the scientific sectors. Additionally, the ever-growing development of long-range AUVs (Furlong et al., 2012), capable of operating for a large period of time and flying for thousands of kilometers in a single deployment, has pushed the research boundaries of AUVs usage in survey tasks. As a result, regardless of the specific operational area, the design of high-accuracy navigation and localisation systems has arisen as a crucial task in the development of AUV technologies. Indeed, the renowned unavailability of the Global Positioning System (GPS) signal (likewise the whole range of electromagnetic signals) in the underwater domain makes the localisation and navigation goals even more demanding compared to different domains (e.g. air and land).

A range of strategies and approaches have been developed to tackle the AUVs localisation and navigation tasks (Paull et al., 2014). Recently, research in this field has been oriented to the development of adaptive localisation systems rather than customised approaches for specific applications. Acoustic Positioning Systems (APS) (Leonard and Bahr, 2016), with their non-negligible amount of additional hardware to be installed, have been gradually replaced by Inertial Navigation Systems (INS), which rely on the integration of navigation sensor measurements on board the vehicle itself, without the need for external infrastructure. Even though underwater navigation systems are primarily based on bayesian approaches (Allotta et al., 2016; Bar-Shalom et al., 2004), Dead Reckoning (DR) strategies have been proven to be satisfyingly reliable if the available sensors are sufficiently accurate. In particular, DR localisation approaches can provide the vehicle position by integrating, with respect to time, the AUV velocity, which is mostly estimated by exploiting Acoustic Doppler Current Profilers (ADCPs) or Doppler Velocity Logs (DVLs).

* Corresponding author at: Department of Industrial Engineering, University of Florence, via di Santa Marta 3, Florence, 50139, Italy.
E-mail addresses: edoardo.topini@unifi.it (E. Topini), franel@noc.ac.uk (F. Fanelli), alberto.topini@unifi.it (A. Topini), mxp@noc.ac.uk (M. Pebody), alessandro.ridolfi@unifi.it (A. Ridolfi), abp@noc.ac.uk (A.B. Phillips), benedetto.allotta@unifi.it (B. Allotta).
[1] www.isme.unige.it

https://doi.org/10.1016/j.oceaneng.2023.114034
Received 20 December 2022; Received in revised form 10 February 2023; Accepted 19 February 2023
Available online 2 March 2023

However, this specific technique unavoidably leads to position estimate errors, due to the sensor integration drift over time, and, as a consequence, the longer the vehicle mission, the more the position estimate will degrade. Additionally, DR methodologies present the drawback that even a slight fallacy or malfunction in the sensor readings can lead to a remarkable position estimate error and, as a result, a deterioration of the AUV navigation performance. Whilst DVL/ADCP hardware failures are rare, regular operating conditions may result in erroneous or no velocity estimates. To provide a DVL (over ground) velocity estimate, the device must be within bottom lock distance from the seabed. Such range varies depending on many factors (in addition to pure device performance) such as, for instance, the environmental structure and the vehicle speed, but it is not uncommon to reach a maximum range of up to 200 m. Additionally, navigation in mid water column is thus more complex due to convection of the water mass (Salavasidis et al., 2021; Medagoda et al., 2016). While DVL/ADCP can provide a water track velocity estimate (i.e. relative to the water), there must be sufficient particulate in the water column to provide an acoustic return, and in some operating areas this is not the case. In order to address the aforementioned issues, the standard solution for DVL failure patterns relies on the use of the robot dynamical model and the inexorable modelling inaccuracies that do emerge in this nontrivial process. The identification of such a model may indeed prove itself to be considerably challenging, although considerable developments have been carried out over the years for different types of vehicles (Caccia et al., 2000a; Allotta et al., 2018). Additional results have also been achieved by means of expensive Computational Fluid Dynamics (CFD) software to obtain hydrodynamic damping coefficients (Coe, 2013; Phillips et al., 2010). All the mentioned research studies follow the "classical" identification paradigm, that involves techniques to identify parameters of explicitly defined finite-dimensional model structures; more in detail, the traditional methodology consists of using a physics-based model combined with a class of system identification methods to update the parameters of the model. Alternatively, given the ever-increasing availability of underwater domain data (Bernardi et al., 2020), Machine Learning (ML) approaches gained popularity in recent years, where supervised methods were used to estimate the dynamics of a given system without explicit models. For instance, Wehbe (2020) exploited data collected during real AUV experiments to compare several learning methods against standard physics-based approaches. Furthermore, a framework to learn and adapt vehicle models online has been proposed. Regression algorithms, including linear regression, regression trees with different sizes, regression trees ensembles, Gaussian process regression, and support vector machines have been used by Bassam et al. (2022) for estimating ship velocities; in particular, the proposed approach can provide accurate predictions of ship speed under real operational conditions with the aim of optimising ship operational parameters. Moreover, while Gaussian Processes (GP) can be properly exploited for underwater vehicle identification with a low amount of data (Ramirez et al., 2022), the interest in Deep Neural Networks (DNNs) significantly increased in the case of large datasets. In this context, using experimental data from several AUV missions (and/or simulations), a Neural Network (NN) data-driven model can be trained to learn the vehicle motion.

Inspired by these motivations, the main contribution of this work focuses on testing several state-of-the-art DL-based strategies to aid underwater navigation, proposing a solution able to estimate linear velocities without directly exploiting DVL measurements. The authors especially wish to point out that the major design guideline behind this research activity does not rely on replacing the DVL sensor; conversely, the tested promising framework, based on a cutting-edge technology (such as NNs), aims at providing estimates of the vehicle speed where the DVL performance cannot be ensured. Besides, employing an augmented set of devices able to provide navigation information represents an intrinsic boost in redundancy, preventing failures due, for example, to underwater sensor-denied scenarios (such as when the vehicle is far from the seabed or when environmental disturbances – such as bubbles – are present).

The results of this study were obtained by employing AUV navigation data gathered during several missions carried out by the National Oceanography Centre (NOC) in Loch Ness (UK) in November 2021. Firstly, the experimental comparison involved the information provided by Autosub Long Range (ALR) (Roper et al., 2021), a long-range, long-endurance AUV capable of operating for several months and travelling thousands of kilometers in a single deployment, and, as a consequence, requiring a dedicated, accurate and robust on-board localisation system. Subsequently, the proposed methodology was tested on Autosub5 (formerly known as Autosub2000 Under Ice, A2kUI) (Phillips et al., 2020), a recently developed AUV which complements the low-power, long-range capabilities of ALR with a range of high-power acoustic and optical payload sensors. During the above-mentioned tests, the vehicles navigated by means of a standard DVL-based DR strategy and the proposed solution was tested and validated offline. In particular, while this specific work focuses on post-processed data, a testing framework as close as possible to the on-board real online Guidance, Navigation and Control (GNC) subsystems was adopted (Munafo et al., 2019). Finally, considering the quality of the obtained results, on-line underwater tests will be carried out in the near future during experimental campaigns.

This paper is organised as follows: firstly, works related to the usage of NNs for the underwater navigation task are described in Section 2, whereas Section 3 introduces the adopted notation used to model AUV motion. Section 4 is dedicated to the illustration of the proposed methodology by accurately outlining the novelties of the developed architecture in comparison with the standard DVL-based DR approach. In particular, this work focuses on using several NNs in order to estimate AUV linear velocities, without exploiting DVL readings in the inference stage, resulting in a DL-based DR strategy. Section 5 describes the NOC AUVs (and the on-board devices) used to collect data during the Loch Ness trials. Section 6 presents the obtained experimental results and proposes a quantitative analysis of the achieved outcomes. Finally, Section 7 summarises the achieved results and briefly describes future trends as well as applications.

2. Related work

The application of Deep Learning (DL) in the field of marine robotics is still relatively scarce. For instance, several works have been proposed in the context of Automatic Target Recognition (ATR), where the key idea is to find and recognise an object of interest in either visual or acoustic images by using Convolutional Neural Networks (CNNs) (Palomeras et al., 2022; Zacchini et al., 2020; Valdenegro-Toro, 2017). Additional studies explored the usage of Recurrent Neural Networks (RNN) for fault diagnosis of underwater thrusters (Nascimento and Valdenegro-Toro, 2018). In Dimitrov et al. (2021) a Long Short-Term Memory Network (LSTM) has been exploited to create a model of a marine vehicle, with the aim of filling the simulation-to-reality dynamic gap. Moving to the localisation task, several articles have addressed neural networks in order to estimate the motion of marine crafts. Skulstad et al. (2019) accurately presents a DL-based approach to dead-reckoning navigation of dynamically positioned ships; in particular, thruster force demands combined with heading measurements have been used to train a RNN network for aided-navigation tasks. In Li et al. (2020) a nonlinear autoregressive neural network is presented to support the localisation system in the case of a DVL malfunction; the specific model was tested and validated on a ship with a DVL mounted on the vessel hull. Furthermore, Mu et al. (2019) research was focused on the employment of a Hybrid Recurrent Neural Network (HRNN) to estimate AUV positions; to verify the effectiveness of the proposed navigation algorithm, a series of evaluations have been carried out, based on the navigation data collected during real experimental campaigns, comparing the proposed DL-based localisation solution with

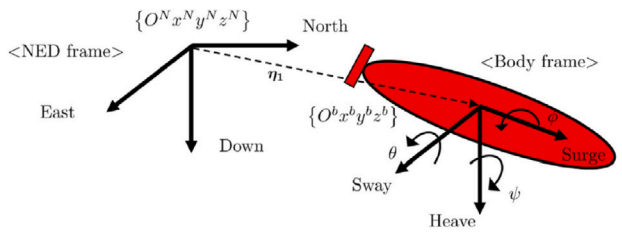

Fig. 1. The SNAME notation.

the Kalman Filters (KFs) -based estimators. Similar studies were also presented in Zhang et al. (2020), Saksvik et al. (2021), Topini et al. (2020), where the data from several sensors (e.g. Inertial Measurement Unit, pressure sensor, and DVL) were exploited as inputs of dedicated RNNs which predict vehicle velocities and positions; the proposed neural network approaches were compared with the AUV on-board navigation system during a series of surveys or in simulations.

3. AUV kinematics and dynamics

The following notation is employed in the context of this work. A generic vector $\boldsymbol{p} \in \mathbb{R}^3$, expressed in a particular $\{O^0 x^0 y^0 z^0\}$ frame is indicated with ${}^0\boldsymbol{p}$. A generic rotation matrix $R \in \mathbb{SO}(3)$ is denoted with two indices R_i^j, where the notation represents the unit vectors of the frame i with respect to frame j. Furthermore, the state of an underwater vehicle – considered as a rigid body – is represented by using two reference frames, by following the Society of Naval Architects and Marine Engineers (SNAME) notation. More specifically, a local Earth-fixed reference frame (assumed as inertial) with axes pointing North, East, and Down (NED frame) $\{O^N x^N y^N z^N\}$, and a right-handed body reference frame $\{O^b x^b y^b z^b\}$ whose origin is the centre of mass of the vehicle (see Fig. 1) with its x-axis pointing in the forward motion direction, its z-axis pointing down, and its y-axis completing a right-handed reference frame. The pose of a vehicle is therefore represented with

$$\boldsymbol{\eta} = \begin{bmatrix} {}^N\boldsymbol{\eta}_1^T & \boldsymbol{\eta}_2^T \end{bmatrix}^\top \quad , \tag{1}$$

where ${}^N\boldsymbol{\eta}_1$ is the position of O^b with respect to the NED frame, and $\boldsymbol{\eta}_2$ is the orientation the body-fixed frame w.r.t. the NED frame, where roll (ϕ), pitch (θ), and yaw (ψ) (RPY) angles are used to describe the orientation. Additionally, the AUV linear and angular velocities along the axis of the body-fixed reference (surge, sway, and heave motion) can be denoted with

$$\begin{aligned} \boldsymbol{\nu} &= {}^b\boldsymbol{\nu} = \begin{bmatrix} {}^b\boldsymbol{\nu}_1^T & {}^b\boldsymbol{\nu}_2^T \end{bmatrix}^\top \\ \boldsymbol{\nu}_1 &= {}^b\boldsymbol{\nu}_1 = [u\ v\ w]^\top \\ \boldsymbol{\nu}_2 &= {}^b\boldsymbol{\nu}_2 = [p\ q\ r]^\top \end{aligned} \quad . \tag{2}$$

The differential kinematic model is illustrated in Eq. (3), and further information can be found in Antonelli (2018):

$$\begin{aligned} \dot{\boldsymbol{\eta}} &= J(\boldsymbol{\eta})\boldsymbol{\nu} \\ \begin{pmatrix} {}^N\dot{\boldsymbol{\eta}}_1 \\ \dot{\boldsymbol{\eta}}_2 \end{pmatrix} &= \begin{bmatrix} R_b^N(\boldsymbol{\eta}_2) & 0_{3\times3} \\ 0_{3\times3} & T_b^N(\boldsymbol{\eta}_2) \end{bmatrix} \begin{pmatrix} {}^b\boldsymbol{\nu}_1 \\ {}^b\boldsymbol{\nu}_2 \end{pmatrix} \quad , \end{aligned} \tag{3}$$

where R_b^N is the rotation matrix between the body and the NED frame, and $T_b^N(\boldsymbol{\eta}_2)$ is the matrix mapping the angular velocity ${}^b\boldsymbol{\nu}_2$ onto the derivatives of the orientation angles.

Regarding the complete dynamic model of a marine vehicle in absence of marine currents (Fossen, 1994), the equation describing the forces acting on the centre of mass is:

$$M\dot{\boldsymbol{\nu}} + C(\boldsymbol{\nu})\boldsymbol{\nu} + D(\boldsymbol{\nu},\boldsymbol{\delta})\boldsymbol{\nu} + \mathbf{g}(\boldsymbol{\eta}) = \boldsymbol{\tau}(\boldsymbol{\nu},\boldsymbol{n}_p,\boldsymbol{\delta}) \quad , \tag{4}$$

where M indicates the mass matrix, $C(\boldsymbol{\nu})$ describes the centrifugal and Coriolis matrix, $D(\boldsymbol{\nu},\boldsymbol{\delta})$ are the damping matrix, $\mathbf{g}(\boldsymbol{\eta})$ reports the effects of gravity and buoyancy, $\boldsymbol{\tau}(\boldsymbol{\nu},\mathbf{n}_\mathbf{p},\boldsymbol{\delta})$ indicates the forces and torques provided by the rotational speeds $\boldsymbol{n}_p$ of m propellers and by the vehicle's control planes whose angular positions are stored in $\boldsymbol{\delta}$, $\boldsymbol{\eta}$ and $\boldsymbol{\nu}$ are as defined in Eq. (3).

4. Proposed methodology

Broadly speaking, the suggested architecture is composed of two hierarchical phases: firstly, in an offline learning stage, the NNs are trained by employing the data collected from the vehicle during missions. Subsequently, the prediction values, supplied by the NNs, are exploited together with the estimated AUV attitude in standard DR velocity-integration strategies.

4.1. Dead reckoning navigation system

For what concerns AUVs overall navigation system, a parallel structure decoupling the attitude and position estimates is commonly exploited (Costanzi et al., 2016; Salavasidis et al., 2019). In particular, the AUV orientation is usually estimated using Inertial Measurement Units (IMUs), magnetic compasses, or high-precision Attitude and Heading Reference Systems (AHRS) exploiting ring laser or fibre optic gyroscopes. On the other hand, the standard DR methods usually estimate the AUV position by integrating the linear velocity measured with highly-accurate instruments such as DVLs or ADCPs. In particular, a DR-based position update is shown in Eq. (5):

$$\boldsymbol{\eta}_1(t_{k+1}) = \boldsymbol{\eta}_1(t_k) + \boldsymbol{R}_B^N(\boldsymbol{\eta}_2(t_k))\,\boldsymbol{\nu}_1(t_k)\,\Delta t \quad , \tag{5}$$

where, following the notations introduced in Section 3, $\boldsymbol{\eta}_1(t_{k+1}1)$ and $\boldsymbol{\eta}_1(t_k)$ are respectively the current and previous NED position estimation output of the DR navigation system, $\boldsymbol{\nu}_1(t_k)$ contains the body-fixed frame linear velocities, $\boldsymbol{R}_B^N(\boldsymbol{\eta}_2(t_k))$ represents the rotation matrix between the NED and the body-fixed frames. It is not uncommon to replace the third component of $\boldsymbol{\eta}_1(t_{k+1})$ with a depth estimate computed directly from pressure readings, such as those provided by a Conductivity, Temperature and Depth (CTD) probe.

It is worth noting that the DR procedure commonly provides sufficient short-term accuracy, while uncompensated sensor errors unavoidably introduce an unbounded error in the positioning error. The DR error is a combination of multiple error sources in velocity and heading measurements that can be present throughout the whole mission. While the impossibility of maintaining the bottom lock in DVL-failure scenarios can be the most relevant source of error, there are further DVL bias effects which may affect the sensor readings (function of the flying altitude, seabed properties, or caused by the approximate knowledge of the speed of sound through water).

The approach followed in this paper is to merge, in an innovative approach, the well-established DR methodology with state-of-the-art DL methodologies to estimate the position of an AUV. Indeed, whilst the DR position propagation model of Eq. (5) remains unchanged, the AUV body-fixed linear velocities $\boldsymbol{\eta}_1$ are estimated through the use of NNs in case of the DVL failure. Therefore, the aforementioned vehicle body-fixed linear velocities are provided by means of NN model predictions rather than DVL readings, as illustrated in Fig. 2. It is also important to mention that another strength of the proposed approach is that the inputs used to train the DL models come from the data generated by sensors generally employed on AUVs: this means that no special or bespoke device is required for this approach to succeed, since the required inputs would be available on board anyways.

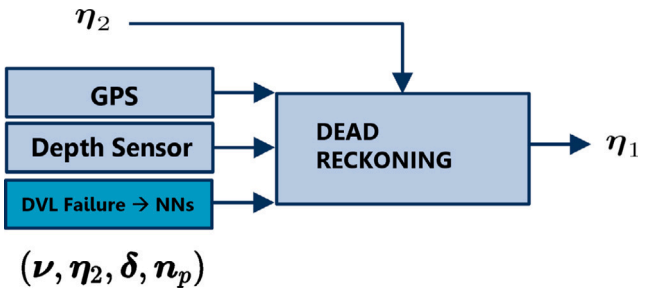

Fig. 2. Proposed DL-based Dead Reckoning architecture in case of DVL failure.

4.2. Deep-learning for model identification

ML methods, and more specifically the DL implementations of the ML theory, have received growing interest over the past decade. This was driven by the unrivalled results obtained through the use of DL technologies in a large range of problems as, for instance, in computer vision and speech recognition applications (Goodfellow et al., 2016), as mentioned in Section 1. As a matter of fact, most of the successful DL applications implement a type of supervised learning where they aim to learn a commonly nonlinear mapping between some observed features X and a corresponding set of targets Y from a dataset of samples $(X,\ Y)$. As far as this specific application is concerned, the key idea is modelling the dynamics of the vehicle, given a dataset provided by the on-board sensor readings. Considering an AUV dynamical system described by Eq. (4), the evolution of linear velocity ν_1 can without loss of generality be expressed in the following form:

$$\dot{\nu}_1 = \mathcal{F}\left(\nu, \eta_2, \delta, n_p\right) \quad . \tag{6}$$

While, on the one hand, Eq. (6) properly describes the AUV dynamics, on the other hand the employment of this model directly (i.e. using the linear body-fixed accelerations $\dot{\nu}_1$ as the target vector) presents several drawbacks. Firstly, the linear body-fixed accelerations are not usually obtainable with a satisfactory degree of reliability (if estimated as the time derivative of DVL velocity measurements, they would be tied to the sampling period of the specific device; if measured by accelerometers, they would be affected by considerable noise). Secondly, the use of acceleration values in a DR-based navigation system requires an additional numerical integration step together with the one needed for the estimation of the AUV position, as reported in Eq. (5), which implies an ever-growing estimation drift. Driven by these consideration, we chose a different approach with the aim of modelling AUV dynamics. In particular, the discrete-time version of Eq. (6) has been considered:

$$\nu_1(t_{k+1}) = \mathcal{F}\left(\nu(t_k), \eta_2(t_k), \delta(t_k), n_p(t_k), \Delta t\right) \quad , \tag{7}$$

where Δt indicates the time step ($\Delta t = t_{k+1} - t_k$). With the model of Eq. (7), the target of the learning phase is the linear velocity at time t_{k+1}, given the inputs at time t_k. It is hence important to discuss how such inputs are obtained. The time step is related to the time period of the navigation system, which is usually constant and will be omitted in the following. Furthermore, we assume that the AUV orientation $\eta_2(t_k)$ is directly estimated from a dedicated system as previously discussed, and that this estimation does not depend on velocities or positions (Costanzi et al., 2016); we also assume that such a system is able to estimate the body-fixed angular velocity ν_2. Similarly, the propeller rotational speeds $n_p(t_k)$ and the control planes displacements $\delta(t_k)$ are assumed to be measured by accurate and independent sensors. However, DVL readings cannot obviously be used for linear velocity estimation, since we are assuming that the proposed methodology is employed in the absence of valid bottom-lock measurements or DVL failure. If available, a basic approximation could be the employment of the water track velocity if the DVL is still operational; nonetheless, this particular strategy can properly work only if marine currents are not too strong, and, as a matter of fact, it lacks generalisation. At the same time, the employment of the estimated value $\hat{\nu}_1(t_k)$ as input, at the previous time step t_k, will lead to an unavoidable drift. Driven by these considerations, we assume that some prior knowledge of the linear velocity, such as the one produced by a physics-based model identified with standard procedures (Caccia et al., 2000a; Wehbe, 2020), is available. Note that we do not require such model to be accurate, but only to provide a first approximation of the linear velocity of the vehicle. Additionally, the same dataset used for training the NN can be employed in the identification of the model.

In detail, let $\tilde{\nu}_1 \in \mathbb{R}^3$ be a body-fixed linear velocity vector estimated from a generic physics-based AUV model, the goal of the optimisation process is to minimise the following loss function

$$\mathcal{L} = \sum_{t=1}^{T} \frac{1}{T} \left\| \nu_1 - \mathcal{F}\left(\nu_2, \tilde{\nu}_1, \eta_2, \delta, n_p, W\right) \right\|^2 \quad , \tag{8}$$

where t and T are respectively the time step and the length of the training data, W is the set of weight and bias parameters of the chosen DL model. The key idea is to investigate whether it is possible to use a mixed strategy with a Deep Learning-based approach taking as inputs also the values estimated by a physics-based model, improving the accuracy and generalisation of the results. In particular, the supervised learning problem defined by the minimisation of the function in Eq. (8) can be tackled by employing one of the state-of-the-art NNs which, at the end of the optimisation process, predicts the body-fixed surge velocity at the current time step.

In the context of this work, four different NNs have been evaluated to solve the regression problem in Eq. (8):

- Multi-Layer Perceptron (MLP), which can be seen as a nonlinear generalisation of a linear model;
- LSTM, as recent studies have outlined their usefulness (Hochreiter and Schmidhuber, 1997) in performing robust sequence learning, where a correlation exists between one sample and a few others preceding it;
- CNNs, as they emerged as a relevant tool for time series prediction in multiple parallel inputs and multi-step forecasting cases;
- Convolutional Long Short-Term Memory Recurrent Neural Networks (C-LSTM), where CNNs are used as a stacked component within an LSTM network.

For an in-depth discussion about deep learning and the cited NNs, the reader may refer to Goodfellow et al. (2016).

5. AUV platforms and dataset acquisition

As already introduced in Section 1, the performance of the proposed DL-based DR strategy has been evaluated and validated offline by employing the navigation data gathered during several missions carried out by the National Oceanography Centre (NOC) in Loch Ness (UK) in November 2021. Firstly, the data gathered by ALR (Roper et al., 2021, 2017), a long-range and long-endurance AUV capable of operating continuously for several months and travelling thousands of kilometers, has been used to validate the approach. Subsequently, the proposed methodology has been tested on Autosub5 (Phillips et al., 2020), a newly developed AUV which complements the low-power, long-range under ice capabilities of ALR with a wide variety of acoustic and optical sensors.

5.1. Autosub long range (ALR) AUV

ALR (Roper et al., 2021, 2017) is a long-range, long-endurance flight-style AUV (see Fig. 3). Long-range autonomy is enabled by ensuring a low hotel load and a relatively slow cruise speed. Propulsion

Fig. 3. ALR4 during the trials in Loch Ness (UK), November 2021.

Fig. 4. Autosub5 being deployed in Loch Ness (UK), November 2021.

power is provided by a single custom-designed propulsion unit which drives a rear two-bladed propeller. The vehicle is also manoeuvred using two stern planes and a rudder controlled using custom actuators, while the top fin is fixed and contains antennae for GPS, WiFi and Iridium satellite communication. The NOC currently operates six ALRs, three with a 1500 m depth rating, and three rated for 6000 m. Given the restrictions imposed by long-range missions, ALRs are equipped with navigation sensors with low power consumption: a u-blox M8 GPS module to obtain GPS fixes when the ALR surfaces, downward-looking DVL (300 kHz Teledyne RDI Workhorse on the 6000 m rated versions, and 500 kHz Nortek DVL500 on the 1500 m rated vehicles) to estimate the 3D AUV velocity in the body-fixed reference frame, a 6-axis PNI TCM XB compass/attitude module based on magneto-inductive sensors, and a Sea-Bird SBE 52-MP CTD to measure the operating depth. For these experiments, ALR4 (a 1500 m depth rated variant) was used.

5.2. Autosub5 AUV

Autosub5 (Phillips et al., 2020; Consensi et al., 2022) is a conventional work class AUV developed for deep ocean and under ice measurements; the vehicle is equipped with high-power payload sensors used to collect science data such as a Multi-Beam Echo Sounder (MBES), a SideScan Sonar (SSS), a Sub Bottom Profiler (SBP), colour cameras and a Conductivity Temperature and Depth (CTD) senors. The main navigation solution is provided by a Sonardyne SPRINT-Nav700 INS, which includes a downward-looking Sonardyne Syrinx DVL. The vehicle has been designed with redundancy in mind: in the case of failure of the primary navigation system, an independent MEMS IMU combined with CTD depth measurements will be used to take the vehicle to safety. Focusing on the vehicle actuators, Autosub5 has been designed with twin rear thrusters, each capable of providing sufficient thrust to ensure the AUV operates above its minimum cruise speed along the longitudinal AUV motion, and has four individually actuated control surfaces in an 'X' configuration to ensure redundancy (see Fig. 4).

5.3. Model-based navigation aided system

For both vehicle types, the navigation system ensures that the robot can navigate even in the event of a DVL breakdown or malfunction (or simply in the absence of bottom lock), using a physics-based model to provide the navigation system the linear velocity needed in Eq. (5) to estimate the AUV position. In particular, referring to Eq. (4), the following assumptions have been made to model the AUV motion.

Assumption 1. Most of the AUV dynamics takes place in the positive longitudinal direction. As a consequence, the body-fixed sway and heave velocities can be considered equal to zero.

This assumption can be considered valid considering that both ALR and Autosub5 AUVs cannot be controlled in these directions of motion. Both have been designed to perform survey and inspection tasks and they typically navigate on straight line paths in order to minimise the hydrodynamic damping. Consequently, the estimated vehicle body-fixed speed can be approximated in Eq. (5) with Eq. (9):

$$\hat{\boldsymbol{\nu}}_1 = [\hat{u}, 0, 0]^\top \quad , \tag{9}$$

where $\hat{u} \in R$ is the estimate of the body surge speed.

Assumption 2. The inertial, gravitational, centripetal, and Coriolis effects in the AUV model can be neglected.

Although this assumption may seem to be of considerable impact, it should be noted that for vehicles that cannot perform hovering like those described above, an attempt is made to maintain limited instances of acceleration (and deceleration) at the initial dive and final resurfacing phases. In addition, the use of such strategies allows for less battery usage with respect to sudden changes in the vehicle longitudinal speed. In this context, this assumption can be considered valid, and Eq. (4) significantly simplifies as

$$D(\boldsymbol{\nu})\boldsymbol{\nu} = B\mathbf{t}(\boldsymbol{\nu}, \mathbf{n_p}, \boldsymbol{\delta}) \quad , \tag{10}$$

by also using the definition of the TAM, as in Eq. (13).

Assumption 3. The main damping contributions are given by the nonlinear skin friction due to turbulent boundary layers, and by the viscous damping force due to vortex shedding, while the drag related to the stern and the control planes can be neglected. In particular, the non-linearity of the drag terms, adopted by Fossen (1994), Antonelli (2018), Caccia et al. (2000b) is also employed in the context of this work.

Since both vehicles under consideration move at low speed, the coupling between the dissipative effects can be neglected, leading to a diagonal damping matrix. Additionally, it can be noted that quadratic drag terms commonly dominate over the linear ones, and the matrix $D(\boldsymbol{\nu})$ in Eq. (4) can be approximated with

$$D(\boldsymbol{\nu}) = -\operatorname{diag}_{6\times 6}\left\{\cdots X_i|\nu_{1,i}| \cdots X_j|\nu_{2,i}| \cdots\right\} \quad , \tag{11}$$

where $\operatorname{diag}_{n\times n}(\cdot)$ is the operator which builds a n-by-n diagonal matrix from a vector and the scalar $\upsilon_{1,i}$ is the component of the body-fixed velocity vector $\upsilon_{1,i}$ along the ith direction of motion. For the sake of completeness, the first three terms in Eq. (11) can be approximated as

$$D_i\left(\nu_{1,i}\right) = X_i|\nu_{1,i}| = \frac{1}{2}\rho A_{f,i} C_{D,i}\left|\nu_{1,i}\right| \quad , \tag{12}$$

where ρ represents the water density, $A_{f,i}$ is the projection of the area of the hull of the vehicle on a plane perpendicular to the ith axis of the body-fixed frame, and $C_{D,i}$ is the drag coefficient, which quantifies the fluid resistance against the vehicle motion.

Assumption 4. The longitudinal thrust provided by each propeller can be modelled with a quasi-steady model. Moreover, each propeller is properly aligned along the longitudinal motion of the vehicle.

Referring to Eq. (4), a linear relation (Carlton, 2018) holds between forces and moments acting on the vehicle $\boldsymbol{\tau} \in \mathbb{R}^6$ and the thrust $\mathbf{t}$ generated by propellers and control planes,

$$\boldsymbol{\tau}(\boldsymbol{\nu}, \mathbf{n_p}) = B\mathbf{t}(\boldsymbol{\nu}, \mathbf{n_p}, \boldsymbol{\delta}) \quad , \tag{13}$$

where B is the Thrust Allocation Matrix (TAM), which depends on the thrusters and control planes pose with respect to the vehicle's centre of gravity. Regarding the dynamics of a thruster (such as those contributing to the thrust along the direction of forward motion for both ALR and Autosub5), the longitudinal thrust contribution of each propeller t_i is usually obtained from the so-called quasi-steady modelling (Carlton, 2018; Fossen, 1994; Blanke et al., 2000). In detail, each thrust force t_i is computed as a function of a gain K_t and the rotational speed of the ith propeller $n_{p,i}$,

$$t_i = K_t(J_0)\rho D^4 n_{p,i}|n_{p,i}| \quad , \tag{14}$$

where J_0 is called the advance ratio, ρ is the water density and D is the diameter of the propeller. Within the context of this work, we consider that the K_t is constant and is not depending on the axial flow velocity (i.e. respecting the "bollard" condition). Referring to the second part of the assumption, the propellers on both ALR and Autosub5 have been fixed along the surge direction of motion in both vehicles (and they are the only actuators contributing to the thrust in that direction). Consequently, the body-fixed force along the surge axis can be calculated as the sum of each thrust contribution.

Driven by these considerations, and by using Eqs. (10) and (12), a physics-based model used to estimate the surge body-fixed speed can be defined as

$$\hat{u} = k_p \sqrt{\sum_{i=1}^{m} n_{p,i}|n_{p,i}|} \quad , \tag{15}$$

where m is the number of the thrusters, k_p is the propeller model coefficient which includes the constant terms in Eqs. (14). The resulting estimate of the body-fixed surge velocity $\hat{u}$, introduced in Eq. (9), is employed in the standard DR strategy defined in Eq. (5). Finally, it is worth noting that in the case the AUV has been provided with only one propeller, as, for instance, ALR, Eq. (15) simplifies in such a way that a linear relationship holds between the propeller rotational speed and the AUV body-fixed surge velocity. Even though the authors are aware that the proposed physics-based model results over-simplified compared to the "true" vehicle dynamics, the key idea is to test the feasibility of our approach (previously described in Section 4) with a model which requires a basic identification procedure. Indeed, the model based on Eq. (15) requires only two different datasets: the surge body-fixed velocity provided from the DVL, and the propeller rotational speeds, which are usually measured by sensors directly placed on the propeller shafts by the manufacturer.

Moving to the DL-based strategy, Eq. (8) and its continuous-time counterpart Eq. (6) can be simplified by considering the characteristics of the considered vehicles: indeed, we can disregard angular velocity (the vehicles move and turn slowly), and sway and heave velocities and roll (they are not actively controlled and by design the vehicles will likely not move in those directions unless subject to external forces); at the same time, heading is irrelevant for our problem. For ALRs and Autosub5, Eq. (6) can be finally simplified as follows:

$$\dot{u} = \mathcal{F}\left(u, \boldsymbol{\nu}_2, q, \boldsymbol{\delta}, \boldsymbol{n}_p\right) \quad , \tag{16}$$

which leads to the minimisation of the following function:

$$\mathcal{L} = \sum_{t=1}^{T} \frac{1}{T} \left\| u - \mathcal{F}\left(\tilde{u}, \boldsymbol{\nu}_2, q, \boldsymbol{\delta}, \boldsymbol{n}_p, W\right) \right\|^2 \tag{17}$$

where we recall that $q \in \mathbb{R}$ is the pitch value defined in Eq. (3), $\tilde{u}$ is the value of the surge body-fixed speed estimated by the propeller model, and the control planes vector $\boldsymbol{\delta}$ dimension changes depending on the vehicle (i.e. two for ALR, which is equipped with a rudder and a stern plane, four for Autosub5 given its independently controlled control planes, as described in Sections 5.1 and 5.2).

6. Experimental results

The results reported in this section use the navigation data collected during several missions performed in Loch Ness (UK) in November 2021. Loch Ness is 36 km long and approximately 2.7 km wide for the majority of its length, the centre of the Loch is 220 m deep. Experiments were conducted in the vicinity of Urquhart Bay. The flow through the Loch is slow, however, wind driven currents of up to 0.1 m/s were observed during the experiments. Firstly, experimental data from ALR have been employed to test the proposed methodology; subsequently, the whole framework has been evaluated with Autosub5 data. Each mission dataset is composed of several fields, related to the different sensors values, sampled at 1 Hz frequency by the on-board logger. The vehicles relied on the sensors described in Sections 5.1 and 5.2 for the extent of the missions and they performed the required navigation tasks exploiting DVL bottom lock for the entire duration of the missions.

6.1. Training process and scoring metrics

In this study, we employ four different learning methods, namely MLP, LSTM, CNN, and C-LSTM. For the implementation of the aforementioned NNs, we used the TensorFlow Deep Learning library (Abadi et al., 2015) for inference and training phases. Referring to the latter, we decided to employ the Keras (Chollet et al., 2015) framework, which provides a hands-on usage of neural networks, by sequentially stacking different state-of-the-art layers. More specifically, the following models have been used in the context of this work:

- MLP: the MultiLayer Perceptron model is created by stacking a certain number of Fully-Connected (FC) layers, where each one contains a predefined number of neurons, and a non-linear activation function;
- LSTM: as in the previous case, the model is composed by several Long Short-Term Memory Network (Hochreiter and Schmidhuber, 1997) layers stacked together;
- CNN: the Convolutional Neural Networks are defined as having one or more 1D convolutional stacked layers (each one provided with feature maps and a kernel size value) followed by a pooling layer which reduces the dimensionality of the feature maps;
- C-LSTM: the Convolutional Long Short-Term Memory Recurrent Neural Networks, where CNN and LSTM layers are stacked together. The key idea of this architecture is merging the monodimensional convolutional layer ability for feature extraction on input data, combined with LSTMs to support sequence prediction.

It is worth mentioning that a fully connected layer is also added after the stacked layers in the LSTM, CNN and C-LSTM networks, in order to ideally provide a "buffer" before making a prediction. Finally, each DL model architecture has been paired with a regularising-oriented dropout layer alongside a fully connected layer, which translated the output of the stacked layers into the monodimensional predicted velocity values, followed by a linear activation function. A graphical representation of the described models can be observed in Fig. 5 (a–d), where the standard configurations (only one stacked layer is added in each model) of MLP, LSTM, CNN and C-LSTM for solving monodimensional regression problems are illustrated. Nevertheless, deeper architectures can be developed by employing a larger values of stacked layers.

A cross-validation strategy with a grid search map has been exploited for each different NN in order to tune the parameters. More

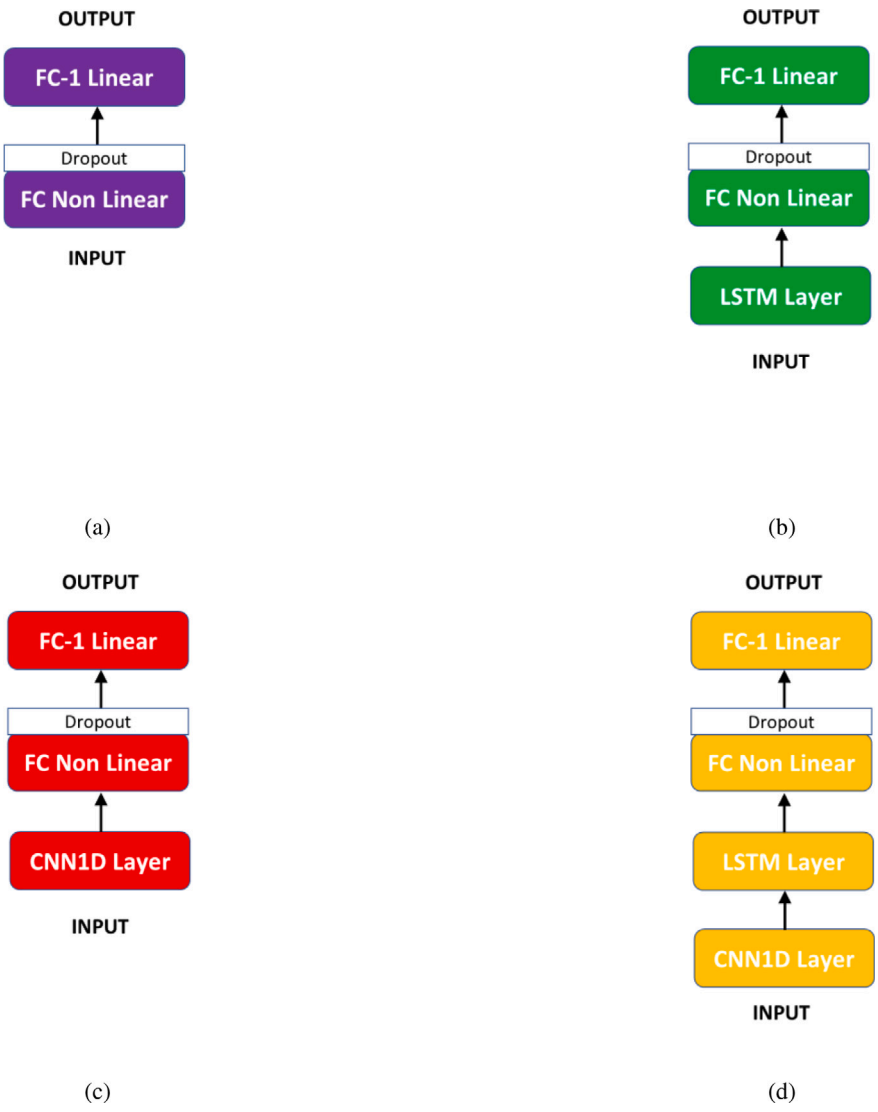

Fig. 5. The standard NN architectures defined by sequentially stacking different Keras layers (Chollet et al., 2015): in detail, the MLP (a), LSTM (b), CNN (c), C-LSTM (d) are shown.

specifically, a scheme known as *k-fold cross-validation* has been used to evaluate different hyper-parameter settings for each estimator. The key idea is to split the training data into k subsets, then the model is trained with k - 1 sets and evaluated with the remaining set. This procedure is repeated for k times, leaving a different subset for validation every time, as suggested in Wehbe (2020).

Regarding the time sequence input dimensionality, several tests were conducted leading to select 10-sample sequences (i.e. temporal sequences of ten seconds) for the CNN, LSTM, and C-LSTM; conversely, only the inputs at the previous time step are considered with the MLP, which is not usually employed for time series regression problems. Coherently with the standard regression loss metrics, the NNs have been trained to minimise the Mean Squared Error (MSE) between the target body-fixed surge velocities and their predicted values. For the optimiser and the batch size selection, the NNs have been trained by using the Adam optimiser (Kingma and Ba, 2014) and batch size equal to 1; additionally, a dedicated learning rate scheduler is implemented that adjusts the learning rate between epochs as the training progresses. Even though a number of 1000 epochs had been employed for the whole training, we introduced the early stopping technique on the validation loss in order to avoid undesirable overfitting. Moving to a more detailed overview of the collected dataset, each interested physical quantity has been further normalised to speed up the learning procedure as well as lead to faster convergence.

Moving to a quantitative analysis of the obtained results, to quantify the quality of predictions of a certain model, a scoring method is usually selected. While several scoring metrics can be used for regression problems, the authors decided to focus on the Mean Absolute Error (MAE) and the Mean Absolute Percentage Error (MAPE), defined as follows: let y be the target value, $\hat{y}$ its predicted value, and n the number of samples; then, the following metrics can be defined:

- Mean Absolute Error (MAE):

$$\mathrm{MAE} = \frac{1}{n}\sum_{i=1}^{n}\left|y_i - \hat{y}_i\right| \quad , \tag{18}$$

- Mean Absolute Percentage Error (MAPE):

$$\mathrm{MAPE} = \frac{100\%}{n}\sum_{i=1}^{n}\left|\frac{y_i - \hat{y}_i}{y_i}\right| \quad . \tag{19}$$

In particular, the MAPE has been chosen in order to compare the results for the two different vehicles, reported in the following.

Table 1
Best hyper-parameters estimated with the cross-validation strategy.

Estimator	Best Hyper-parameters
MLP	FC Layers: 1 FC Units: 16 FC Activation function: Hyperbolic tangent
LSTM	LSTM Layers: 1 LSTM Units: 32 FC Layers: 1 FC Units: 8 FC Activation function: Hyperbolic tangent
CNN	CNN Layers: 1 CNN Kernel Size: 3 CNN Feature Maps: 16 FC Layers: 1 FC Units: 8 FC Activation function: Hyperbolic tangent
C-LSTM	CNN Layers: 1 CNN Kernel Size: 3 CNN Feature Maps: 16 LSTM Layers: 1 LSTM Units: 32 FC Layers: 1 FC Units: 8 FC Activation function: Hyperbolic tangent

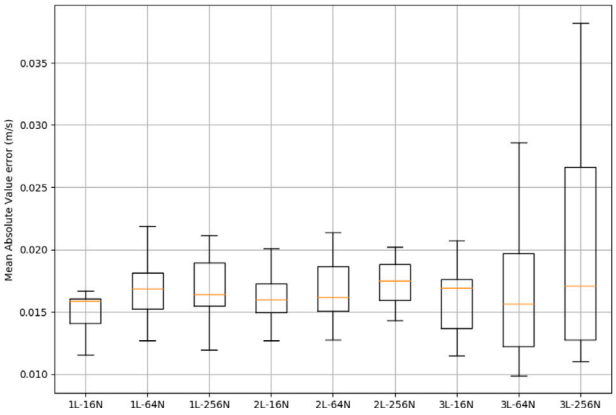

Fig. 6. The MLP cross-validation results for a grid search map of $[1, 2, 3]$ layers composed by $[16, 64, 256]$ neurons. The model with i layers and j neurons has been labelled as iL-jN in the plot.

6.2. Case study 1: Autosub long range

Experimental data from Autosub Long Range was used for the initial validation of the proposed approach. A specific TRaining Mission (TRM), whose data was then used in the training process of the NNs, was planned using NOC's Oceanids C2 command and control infrastructure (Harris et al., 2020). Referring to Fig. 7, the TRM is composed of reciprocal tracks between two different waypoints (approximately 530 meters distance) with the AUV flying at a constant altitude of 40 meters from the lochbed. Different body-fixed surge demands were set in order to provide a dataset as heterogeneous as possible (see Fig. 8), and to avoid overfitting a specific use case with a constant longitudinal speed. Additionally, the data in Figs. 8 and 9 were also used for the estimation of the Propeller Model (PM) as defined in Eq. (15).

The results of the cross-validation strategy described in Section 6.1, are reported in Table 1, in which the parameters of each different NN can be observed.

It can be observed from Table 1 that the best models are quite simple, and neural networks with too deep architectures were not necessary. While not too complex NNs have the significant advantage of being deployed into the vehicle without real time constraint issues, a careful reader may wonder whether better performances could bee achieved with deeper network architectures. Motivated by these considerations, the authors report the comparison among several NN parameters obtained from the cross validation strategy. For the sake of brevity, only the results of the MLP cross-validation approach have

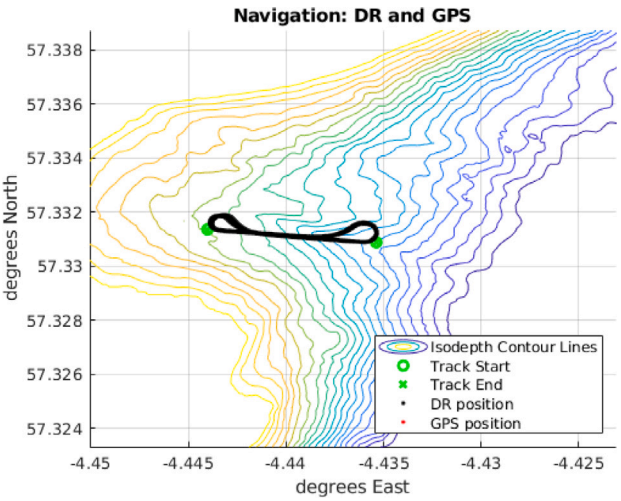

Fig. 7. The trajectory of the ALR TRM.

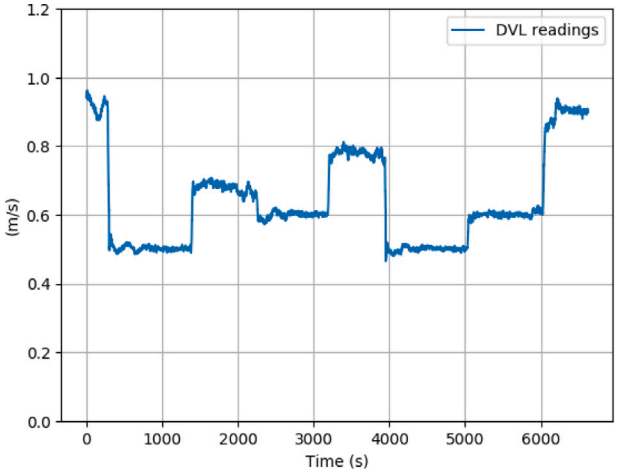

Fig. 8. The DVL readings for the ALR TRM.

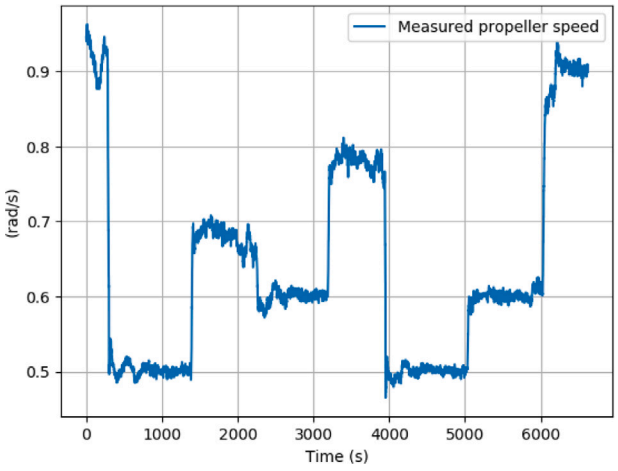

Fig. 9. The measured propeller speed for the ALR TRM.

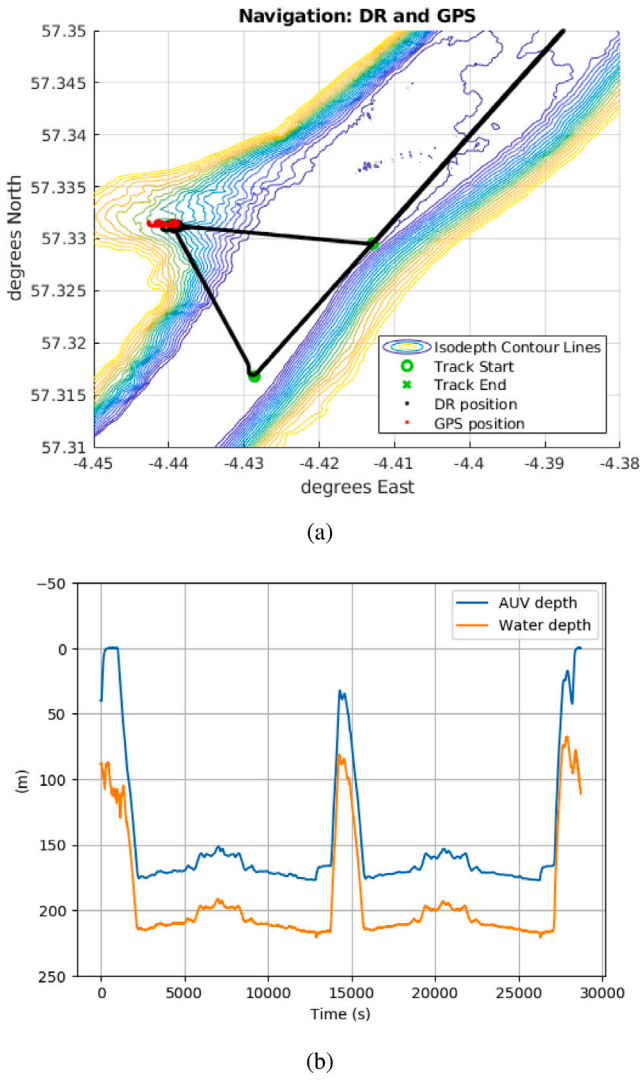

Fig. 10. The trajectory (a) and the depth (b) of the ALR TEM1.

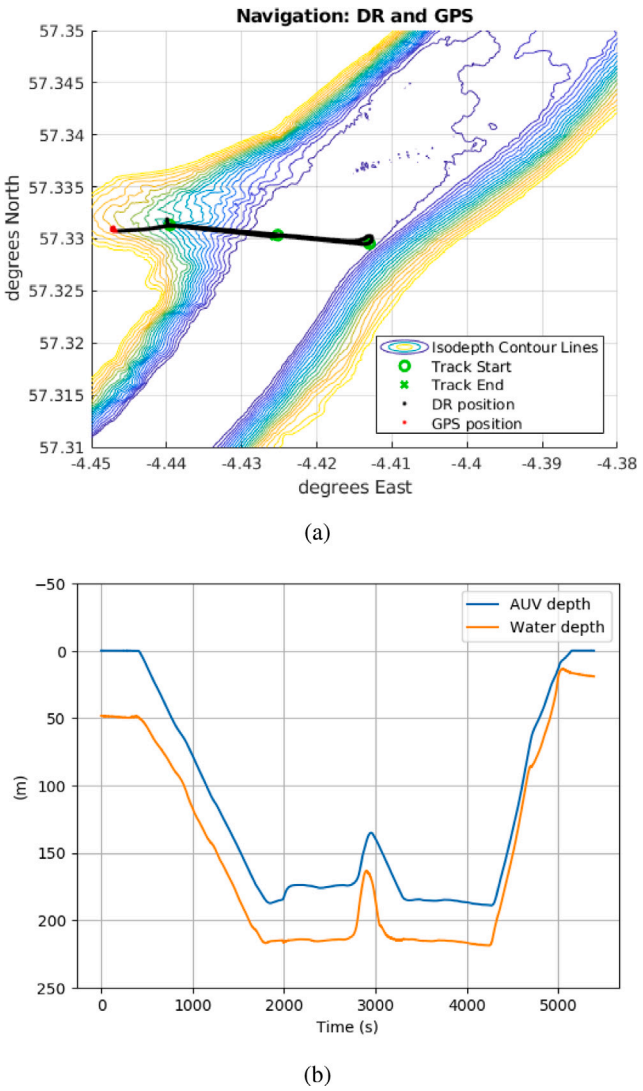

Fig. 11. The trajectory (a) and the depth (b) of the ALR TEM2.

been reported in the manuscript. Nonetheless, the same methodology has been applied to the other NNs employed in the context of this work and equivalent patterns do arise. Referring to the specific MLP cross-validation, we increased both the number of the stacked layers and the values of units for each layer, and every network is trained several times with random weight initialisation. It is worth noting that also different activation functions and dropout values have been tested, but omitted in Fig. 6 since they do not significantly contribute to the performance of networks with deeper architectures. Thus, the validation mean absolute error and standard deviation of each neural network are calculated, and can be observed in Fig. 6, where each MLP model with i layers composed by j neurons has been labelled as iL-jN in the plot.

From a quantitative point of view, it can be observed that no practical improvements are obtained with a "bigger" architecture. In particular, while the first seven models are quite comparable in Fig. 6, the last two present a relevant increase in the standard deviation. In this context, the standard deviation of a model can be considered a robustness index of the used estimator: a low variance indicates that the estimator is able to achieve robust performance when trained and evaluated in different splits of the data. Conversely, it is worth noting that deeper architectures might lead to slightly overfitted models, whenever complex layouts are not needed to learn the target values.

Moving to the test dataset, four different TEst Missions (TEMs) were used to test the neural networks on unseen data. For the sake of brevity, the reader can observe two of the TEMs paths in Figs. 10–11 (a), as estimated by the on-board ALR localisation algorithms. When the vehicle is on the surface, the position is estimated by employing GPS measurements; while ALR is underwater, its position is estimated by using a DR approach as described in previous sections. It is essential to remark that each test mission was not included in the training and validation dataset and, thus, can be adopted as an adequate unknown scenario for the test phase. Additionally, we did not specifically plan the TEMs for the identification procedure, but instead used missions whose characteristics reflect what the vehicle can realistically be asked to do during survey tasks. In detail, each TEM is composed of different tracks between pairs of waypoints with a constant longitudinal cruise speed.

In order to provide a performance analysis, the proposed strategy was compared with the canonical DVL-based DR technique, which, essentially, is used as a ground-truth baseline to validate the novel solution. As a consequence, the target values in Eqs. (18) and (19) are the DVL-measured velocity estimates. As far as quantitative results are concerned, Table 2 shows the obtained results (with the scoring metrics defined in Section 6.1) for the different NNs. Additionally, the results obtained with the physics-based model described in Section 5.3 are also

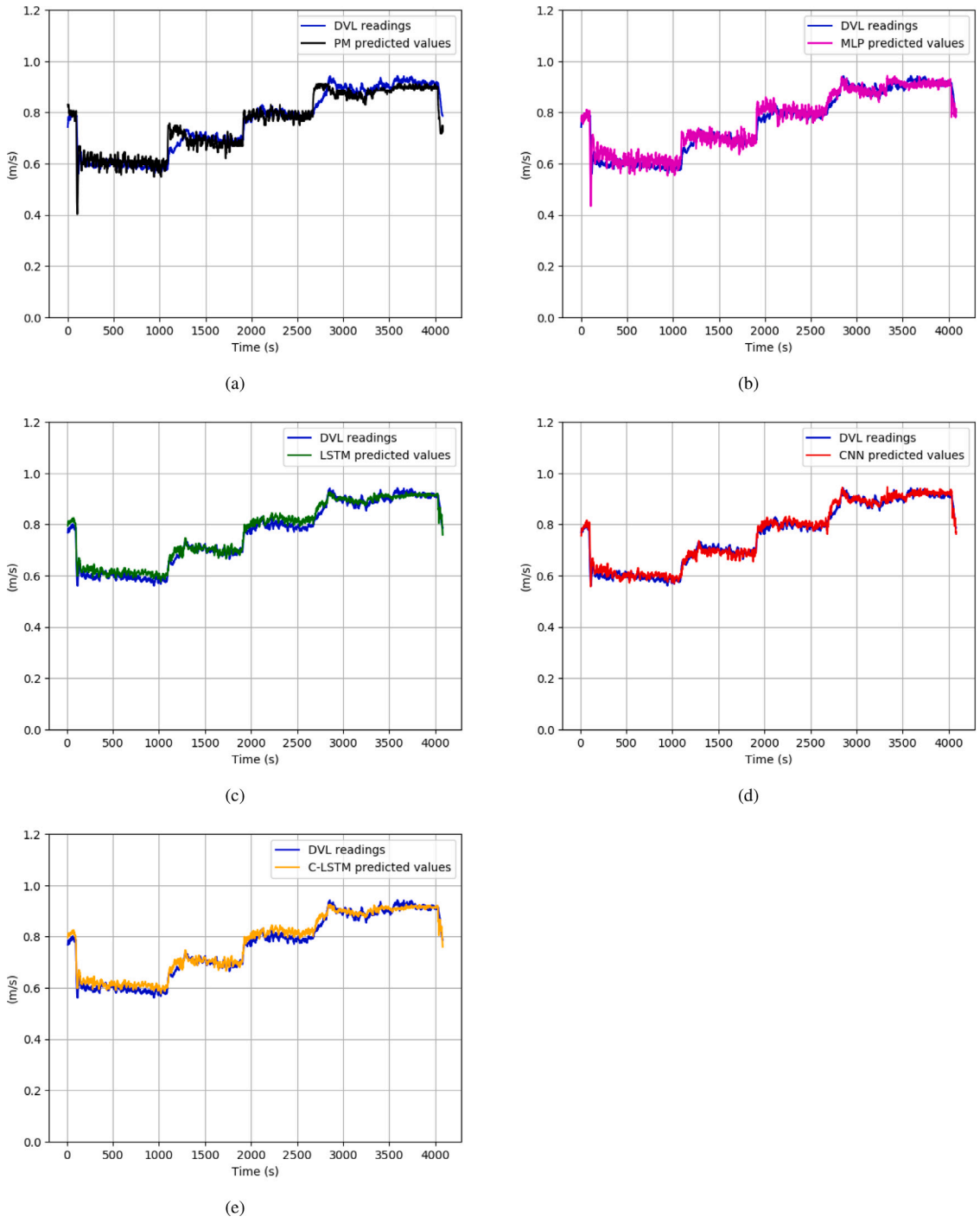

Fig. 12. The results obtained during an ALR TEM. In particular, the predicted body-fixed surge velocities estimated with the Propeller Model (a), MLP (b), LSTM (c), CNN (d), C-LSTM (e) are shown.

reported. Within this context, the PM, defined in Eq. (15), seems to work relatively well for ALR TEMs; this is expected from a vehicle with only one thruster executing missions without any suddenly changing surge speeds. For the sake of brevity, only the results of one of the ALR TEMs are reported in Fig. 12.

In detail, observing Figs. 12 (a–e), it can be noted that, as expected, the proposed approach outperforms the basic PM for every selected NN. From a qualitative point of view, DL-based strategies show a relevant improvement in terms of the smoothness of the predictions as well as the accuracy in the accelerated phases of the mission. In particular, LSTM, CNN, C-LSTM present smoother predicted values compared to MLP, as expected with time-series regression problems.

Referring to the results obtained in Table 2 with the metrics defined in Section 6.1, it can be observed that the MAEs remains relatively low in absolute terms. Furthermore, it can be seen, in percentage terms, how the joint use of the PM and a NN leads to a relevant decrease of the MAPEs.

6.3. Case study 2: Autosub5

Motivated by the results obtained with ALR, the whole framework was extended and validated with the data collected by Autosub5 in the same trials in Loch Ness. A TRM was planned with several surge speed steps, in order to properly model the longitudinal motion at different

Table 2
Scoring metric results for ALR test missions.

	MAE (m/s)	MAPE (%)
MLP	0.020	2.440
LSTM	0.017	2.150
CNN	0.016	1.852
C-LSTM	0.017	2.150
PM	0.028	3.320

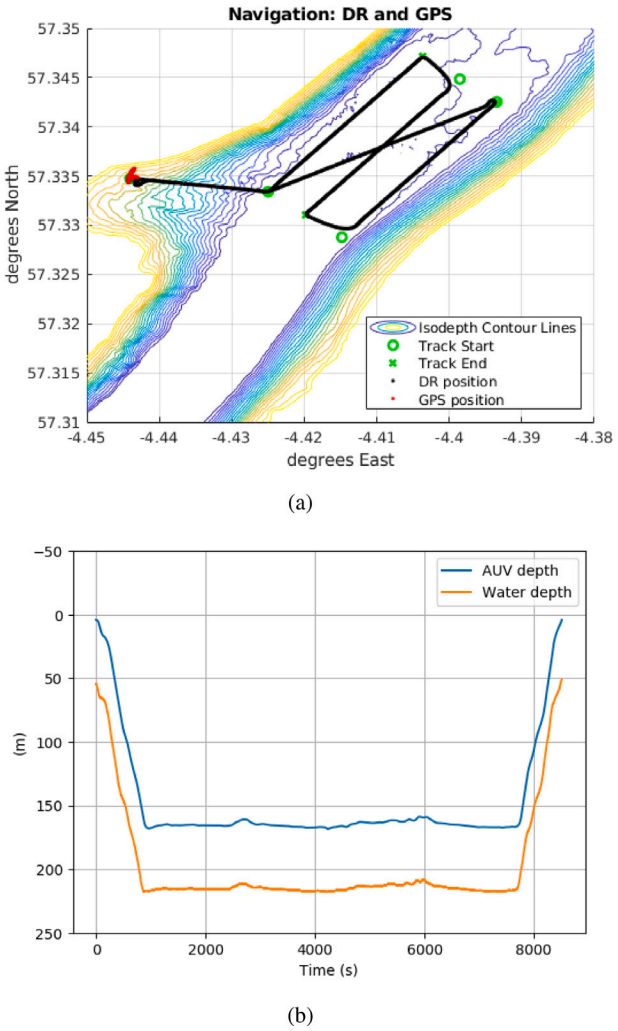

Fig. 13. The trajectory (a) and the depth (b) of the Autosub5 TEM1.

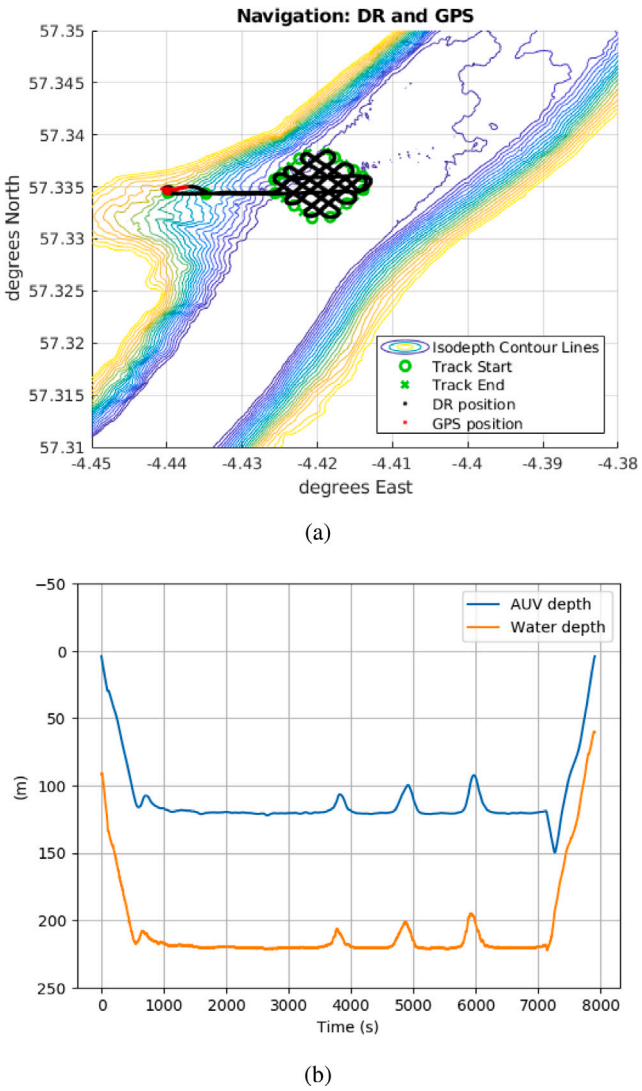

Fig. 14. The trajectory (a) and the depth (b) of the Autosub5 TEM2.

Table 3
Scoring metric results for Autosub5 test missions.

	MAE (m/s)	MAPE (%)
MLP	0.031	2.450
LSTM	0.030	2.348
CNN	0.027	2.078
C-LSTM	0.032	2.518
PM	0.058	4.468

set points. Moreover, as for ALR, four TEMs were used to evaluate the performance of the proposed approach. Differently to the ALR TEMs, we decided to also use two standard lawnmower path missions, in order to test the effectiveness of the developed framework in slightly different types of missions. Coherently with the previous Section, two TEM paths are reported in Figs. 13 and 14, and the estimated surge body-fixed velocities are illustrated in Fig. 15 (a–e). Similar to the ALR case, the joint usage of a physics-based model and NNs outperform the PM estimates. More specifically, referring to 15(a), it is worth noting that the PM is not working particularly well in the second part of the TEM. Conversely, DL-based approaches can mitigate the PM error, resulting in more accurate surge velocity predictions (see Fig. 15 (b–e)).

The scoring metric results for Autosub5 are reported in Table 3. Looking at the PM, it can be observed that the MAE is significantly higher than the ALR one. This result can be explained by taking into account that Autosub5 is equipped with two thrusters and, as a consequence, a PM such as the one adopted in this work is likely to be less accurate in describing the AUV longitudinal dynamics. Conversely, the combination of the PM model as an input to a NN allows to lower the error by almost 50%. Therefore, confirming the results obtained with ALR, it seems that NNs could provide a relevant tool to estimate the unmodelled dynamics of a physics-based model.

6.4. Hardware setup and memory management

Regarding the hardware setup, the training stage was performed on a laptop fitted with 16 GB RAM, an Intel Core i7-8750H processor, and an Nvidia GeForce GTX 2060 card. As already mentioned in Section 1, this specific work focuses on post-processed data; nonetheless, the testing framework adopted a structure as close as possible to the

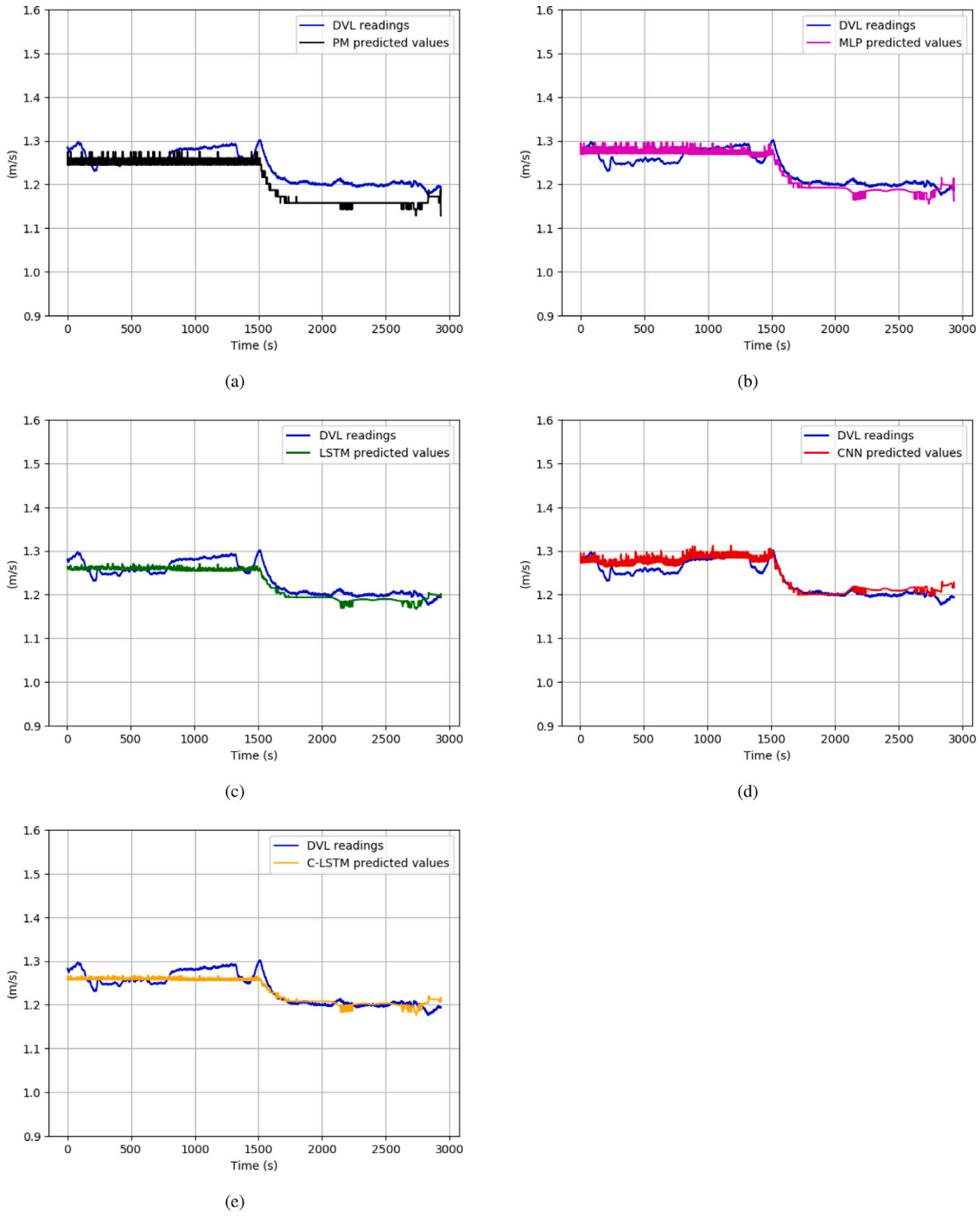

Fig. 15. The results obtained during an Autosub5 TEM. In particular, the predicted body-fixed surge velocities estimated with the Propeller Model (a), MLP (b), LSTM (c), CNN (d), C-LSTM (e) are shown.

components of the real on-board software architecture. In particular, after using the TensorFlow Deep Learning library (Abadi et al., 2015) for the training process and to develop the NN model, the latter was then imported into a suitably developed Robot Operating System (ROS) node to be integrated with NOC's On-board Control System (Munafo et al., 2019) for the inference stage in order to test the feasibility of the proposed approach for online predictions. Being aware that AUV on-board computers are not usually equipped with a GPU, no GPU-based library was used for the offline validation of our approach.

Table 4 shows that the averages of RAM and CPU load over all the missions run with the developed inference methodology are nearly insignificant, suggesting that solving DL-based regression problems directly on-board the vehicle might be feasible. Nevertheless, the authors are aware that several long-range AUVs (Furlong et al., 2012) are equipped with less powerful computers with respect to the one

Table 4
CPU and RAM loads for the inference process.

	CPU LOAD (%)	RAM LOAD (%)
MLP	0.50	0.20
LSTM	0.85	0.30
CNN	0.85	0.30
C-LSTM	0.85	0.30

employed in this offline validation, in order to maintain low or very low energy consumption. Consequently, the numbers obtained in Table 4 might increase if the inference algorithm runs on an AUV computer — although the required computational effort should remain limited. This will be confirmed when the proposed architecture will be tested directly on NOC's AUVs. It is also worth mentioning that no on-board training is involved in our procedure; if training was to be carried out online, a GPU-based board (e.g.the Nvidia GeForce Jetson card) would be strongly recommended.

7. Conclusions and future developments

This paper presents an extended comparison on the use of different NNs to estimate an AUV surge velocity without direct DVL measurements, to be used in a DR-based navigation solution. The proposed approach has been tested and validated using data gathered by NOC ALR and Autosub5 AUVs during in-water trials undertaken in Loch Ness (UK) in November 2021. In particular, the performance of the resulting navigation solution has been evaluated offline using sensors and actuators data collected during a series of in-water missions. NNs trained on the collected data together with a physics-based model obtained by means of a standard identification process are used to improve the accuracy provided by the latter and identify unmodelled dynamics of the vehicle; DVL data logged during the same missions are used as ground truth to provide a quantitative comparison. The results show that the proposed solution largely improves the estimate of body-fixed velocities compared to using a physics-based model alone, for both ALR and Autosub5; furthermore, the estimated CPU load and RAM usage makes this strategy suitable for direct use on board a vehicle without the need for a dedicated processing unit. Finally, the developed strategy has shown the possibility of providing AUVs with fault-tolerant navigation systems, which may rely on a redundant combination of both standard physics-based and DL-based models to increase the accuracy of the available navigation solution.

Future steps will involve online testing of the proposed DL-based DR navigation strategy during field experimental campaigns, with the additional purpose of increasing the size and dimension of the training dataset, providing the trained networks with improved generalisation capabilities. Finally, it is worth mentioning that Deep Learning is an open field of research, and NNs with enhanced performances might be proposed in the next few years; as a consequence, additional tests might be performed to check the feasibility of the proposed approach with cutting-edge DL-based models.

Declaration of competing interest

The authors declare that they have no known competing financial interests or personal relationships that could have appeared to influence the work reported in this paper.

Data availability

Data will be made available on request.

References

Abadi, M., Agarwal, A., Barham, P., Brevdo, E., Chen, Z., Citro, C., Corrado, G., Davis, A., Dean, J., Devin, M., Ghemawat, S., Goodfellow, I., Harp, A., Irving, G., Isard, M., Jia, Y., Jozefowicz, R., Kaiser, L., Kudlur, M., Levenberg, J., Mané, D., Monga, R., Moore, S., Murray, D., Olah, C., Schuster, M., Shlens, J., Steiner, B., Sutskever, I., Talwar, K., Tucker, P., Vanhoucke, V., Vasudevan, V., Viégas, F., Vinyals, O., Warden, P., Wattenberg, M., Wicke, M., Yu, Y., Zheng, X., 2015. TensorFlow: Large-scale machine learning on heterogeneous systems. URL https://www.tensorflow.org/ Software available from tensorflow.org.

Allotta, B., Caiti, A., Costanzi, R., Fanelli, F., Fenucci, D., Meli, E., Ridolfi, A., 2016. A new AUV navigation system exploiting unscented Kalman filter. Ocean Eng. 113, 121–132. http://dx.doi.org/10.1016/j.oceaneng.2015.12.058, URL https://www.sciencedirect.com/science/article/pii/S0029801815007271.

Allotta, B., Costanzi, R., Pugi, L., Ridolfi, A., 2018. Identification of the main hydrodynamic parameters of Typhoon AUV from a reduced experimental dataset. Ocean Eng. 147, 77–88. http://dx.doi.org/10.1016/j.oceaneng.2017.10.032, URL https://www.sciencedirect.com/science/article/pii/S0029801817306406.

Antonelli, G., 2018. Underwater Robots. Springer.

Bar-Shalom, Y., Li, X.R., Kirubarajan, T., 2004. Estimation with Applications to Tracking and Navigation: Theory Algorithms and Software. John Wiley & Sons.

Bassam, A.M., Phillips, A.B., Turnock, S.R., Wilson, P.A., 2022. Ship speed prediction based on machine learning for efficient shipping operation. Ocean Eng. 245, 110449. http://dx.doi.org/10.1016/j.oceaneng.2021.110449, URL https://www.sciencedirect.com/science/article/pii/S0029801821017315.

Bernardi, M., Hosking, B., Petrioli, C., Bett, B.J., Jones, D., Huvenne, V.A.I., Marlow, R., Furlong, M., McPhail, S., Munafo, A., 2020. AURORA, A multi sensor dataset for robotic ocean exploration. IEEE Dataport, http://dx.doi.org/10.21227/nnms-te61.

Blanke, M., Lindegaard, K.-P., Fossen, T.I., 2000. Dynamic model for thrust generation of marine propellers. IFAC Proc. Vol. 33 (21), 353–358. http://dx.doi.org/10.1016/S1474-6670(17)37100-8.

Caccia, M., Indiveri, G., Veruggio, G., 2000a. Modeling and identification of open-frame variable configuration unmanned underwater vehicles. IEEE J. Ocean. Eng. 25 (2), 227–240. http://dx.doi.org/10.1109/48.838986.

Caccia, M., Indiveri, G., Veruggio, G., 2000b. Modeling and identification of open-frame variable configuration unmanned underwater vehicles. IEEE J. Ocean. Eng. 25 (2), 227–240. http://dx.doi.org/10.1109/48.838986.

Carlton, J., 2018. Marine Propellers and Propulsion. Elsevier.

Chollet, F., et al., 2015. Official TensorFlow website. https://github.com/fchollet/keras (Online; Accessed November 2012).

Coe, R.G., 2013. Improved underwater vehicle control and maneuvering analysis with computational fluid dynamics simulations.

Consensi, A., Kingsland, M., Linton, N., Bowring, L., Roper, D.T., Austin-Berry, R., Fairbairn, S., Johnson, A., Morrison, R., Ciaramella, K., Matterson, D., Pebody, M., Williams, V., Fanelli, F., Fenucci, D., Martin, A., Ó hÓbáin, E., Ramdhanie, S., Sherif, R., Morris, A., Phillips, A.B., 2022. Autosub5: Preparing for science. In: IEEE/OES AUV2022. IEEE, pp. 1–6.

Costanzi, R., Fanelli, F., Monni, N., Ridolfi, A., Allotta, B., 2016. An attitude estimation algorithm for mobile robots under unknown magnetic disturbances. IEEE/ASME Trans. Mechatronics 21 (4), 1900–1911. http://dx.doi.org/10.1109/TMECH.2016.2559941.

Dimitrov, M., Groves, K., Howard, D., Lennox, B., 2021. Model identification of a small fully-actuated aquatic surface vehicle using a long short-term memory neural network. In: 2021 IEEE International Conference on Robotics and Automation. ICRA, pp. 5966–5972. http://dx.doi.org/10.1109/ICRA48506.2021.9561454.

Fossen, T.I., 1994. Guidance and Control of Ocean Vehicles. Wiley.

Furlong, M.E., Paxton, D., Stevenson, P., Pebody, M., McPhail, S.D., Perrett, J., 2012. Autosub long range: A long range deep diving AUV for ocean monitoring. In: 2012 IEEE/OES Autonomous Underwater Vehicles. AUV, pp. 1–7. http://dx.doi.org/10.1109/AUV.2012.6380737.

Goodfellow, I., Bengio, Y., Courville, A., 2016. Deep Learning. MIT Press, http://www.deeplearningbook.org.

Harris, C.A., Lorenzo-Lopez, A., Jones, O., Buck, J.J.H., Kokkinaki, A., Loch, S., Gardner, T., Phillips, A.B., 2020. Oceanids C2: An integrated command, control, and data infrastructure for the over-the-horizon operation of marine autonomous systems. Front. Mar. Sci. 7, http://dx.doi.org/10.3389/fmars.2020.00397, URL https://www.frontiersin.org/articles/10.3389/fmars.2020.00397.

Hochreiter, S., Schmidhuber, J., 1997. Long short-term memory. Neural Comput. 9 (8), 1735–1780. http://dx.doi.org/10.1162/neco.1997.9.8.1735.

Kingma, D.P., Ba, J., 2014. Adam: A method for stochastic optimization. http://dx.doi.org/10.48550/ARXIV.1412.6980, arXiv.

Leonard, J.J., Bahr, A., 2016. Autonomous underwater vehicle navigation. In: Springer Handbook of Ocean Engineering. Springer International Publishing, Cham, pp. 341–358. http://dx.doi.org/10.1007/978-3-319-16649-0_14.

Li, W., Chen, M., Zhang, Zhang, L., Chen, R., 2020. A novel neural network-based SINS/DVL integrated navigation approach to deal with DVL malfunction for underwater vehicles. Math. Probl. Eng. http://dx.doi.org/10.1155/2020/2891572.

Medagoda, L., Williams, S.B., Pizarro, O., Kinsey, J.C., Jakuba, M.V., 2016. Mid-water current aided localization for autonomous underwater vehicles. Auton. Robots 40 (7), 1207–1227.

Mu, X., He, B., Zhang, X., Song, Y., Shen, Y., Feng, C., 2019. End-to-end navigation for autonomous underwater vehicle with hybrid recurrent neural networks. Ocean Eng. 194, 106602. http://dx.doi.org/10.1016/j.oceaneng.2019.106602, URL https://www.sciencedirect.com/science/article/pii/S0029801819307279.

Munafo, A., Pebody, M., Consensi, A., Fanelli, F., Fenucci, D., Fox, P., Marlow, R., Prampart, T., 2019. The NOCS on-board control system. In: OCEANS 2019 - Marseille. pp. 1–8. http://dx.doi.org/10.1109/OCEANSE.2019.8867412.

Nascimento, S., Valdenegro-Toro, M., 2018. Modeling and soft-fault diagnosis of underwater thrusters with recurrent neural networks. IFAC-PapersOnLine 51 (29), 80–85. http://dx.doi.org/10.1016/j.ifacol.2018.09.473, URL https://www.sciencedirect.com/science/article/pii/S2405896318321621 11th IFAC Conference on Control Applications in Marine Systems, Robotics, and Vehicles CAMS 2018.

Palomeras, N., Furfaro, T., Williams, D.P., Carreras, M., Dugelay, S., 2022. Automatic target recognition for mine countermeasure missions using forward-looking sonar data. IEEE J. Ocean. Eng. 47 (1), 141–161. http://dx.doi.org/10.1109/JOE.2021.3103269.

Paull, L., Saeedi, S., Seto, M., Li, H., 2014. AUV navigation and localization: A review. IEEE J. Ocean. Eng. 39 (1), 131–149. http://dx.doi.org/10.1109/JOE.2013.2278891.

Phillips, A.B., Kingsland, M., Linton, N., Baker, W., Bowring, L., Soper, S., Roper, D.T., Johnson, A., Morrison, R., Ciaramella, K., Matterson, D., Pebody, M., Marlow, R., Consensi, A., Williams, V., Fanelli, F., Fenucci, D., Martin, A., ÓhÓbáin, E., 2020. Autosub 2000 under ice: Design of a new work class AUV for under ice exploration. In: 2020 IEEE/OES Autonomous Underwater Vehicles Symposium. AUV, pp. 1–8. http://dx.doi.org/10.1109/AUV50043.2020.9267952.

Phillips, A., Turnock, S., Furlong, M., 2010. The use of computational fluid dynamics to aid cost-effective hydrodynamic design of autonomous underwater vehicles. Proc. Inst. Mech. Eng. Part M: J. Eng. Marit. Environ. 224 (4), 239–254.

Ramirez, A.W., Kocijan, J., Leong, Z.Q., Nguyen, H.D., Jayasinghe, S.G., 2022. Dynamic system identification of underwater vehicles using multi-output Gaussian processes. Int. J. Autom. Comput. Eng. 18, 681–693. http://dx.doi.org/10.1007/s11633-021-1308-x, URL https://www.sciencedirect.com/science/article/pii/S0029801821017315.

Roper, D., Harris, C.A., Salavasidis, G., Pebody, M., Templeton, R., Prampart, T., Kingsland, M., Morrison, R., Furlong, M., Phillips, A.B., et al., 2021. Autosub long range 6000: A multiple-month endurance AUV for deep-ocean monitoring and survey. IEEE J. Ocean. Eng. 46 (4), 1179–1191.

Roper, D.T., Phillips, A.B., Harris, C.A., Salavasidis, G., Pebody, M., Templeton, R., Amma, S.V.S., Smart, M., McPhail, S., 2017. Autosub long range 1500: An ultra-endurance AUV with 6000 km range. In: OCEANS 2017-Aberdeen. IEEE, pp. 1–5.

Saksvik, I.B., Alcocer, A., Hassani, V., 2021. A deep learning approach to dead-reckoning navigation for autonomous underwater vehicles with limited sensor payloads. In: OCEANS 2021: San Diego – Porto. pp. 1–9. http://dx.doi.org/10.23919/OCEANS44145.2021.9706096.

Salavasidis, G., Munafò, A., Harris, C.A., Prampart, T., Templeton, R., Smart, M., Roper, D.T., Pebody, M., McPhail, S.D., Rogers, E., Phillips, A.B., 2019. Terrain-aided navigation for long-endurance and deep-rated autonomous underwater vehicles. J. Field Robotics 36 (2), 447–474. http://dx.doi.org/10.1002/rob.21832.

Salavasidis, G., Munafò, A., McPhail, S.D., Harris, C.A., Fenucci, D., Pebody, M., Rogers, E., Phillips, A.B., 2021. Terrain-aided navigation with Coarse maps—Toward an arctic crossing with an AUV. IEEE J. Ocean. Eng. 46 (4), 1192–1212.

Skulstad, R., Li, G., Fossen, T.I., Vik, B., Zhang, H., 2019. Dead reckoning of dynamically positioned ships: Using an efficient recurrent neural network. IEEE Robot. Autom. Mag. 26 (3), 39–51. http://dx.doi.org/10.1109/MRA.2019.2918125.

Topini, E., Topini, A., Franchi, M., Bucci, A., Secciani, N., Ridolfi, A., Allotta, B., 2020. LSTM-based dead reckoning navigation for autonomous underwater vehicles. In: Global Oceans 2020: Singapore – U.S. Gulf Coast. pp. 1–7. http://dx.doi.org/10.1109/IEEECONF38699.2020.9389379.

Valdenegro-Toro, M., 2017. Best practices in convolutional networks for forward-looking sonar image recognition. In: OCEANS 2017 - Aberdeen. pp. 1–9. http://dx.doi.org/10.1109/OCEANSE.2017.8084987.

Wehbe, B., 2020. Long-term adaptive modeling for autonomous underwater vehicles. http://dx.doi.org/10.26092/elib/173.

Zacchini, L., Ridolfi, A., Topini, A., Secciani, N., Bucci, A., Topini, E., Allotta, B., 2020. Deep learning for on-board AUV automatic target recognition for optical and acoustic imagery. IFAC-PapersOnLine 53 (2), 14589–14594. http://dx.doi.org/10.1016/j.ifacol.2020.12.1466, URL https://www.sciencedirect.com/science/article/pii/S2405896320318784 21st IFAC World Congress.

Zhang, X., He, B., Li, G., Mu, X., Zhou, Y., Mang, T., 2020. Navnet: AUV navigation through deep sequential learning. IEEE Access 8, 59845–59861. http://dx.doi.org/10.1109/ACCESS.2020.2982272.